Journal of Power Sources 195 (2010) 5089–5093

Contents lists available at ScienceDirect

Journal of Power Sources

journal homepage: www.elsevier.com/locate/jpowsour

Short communication

Lithium–manganese dioxide cells for implantable defibrillator devices—Discharge voltage models

Michael J. Root*

Cardiac Rhythm Management Research and Development, Boston Scientific Corp., 4100 Hamline Ave. N., St. Paul, MN 55112, USA

ARTICLE INFO

Article history:
Received 10 November 2009
Received in revised form
17 December 2009
Accepted 18 December 2009
Available online 28 December 2009

Keywords:
Batteries
Lithium
Medical
Discharge
Models

ABSTRACT

The discharge potential behavior of lithium-manganese dioxide cells designed for implantable cardiac defibrillators was characterized as a function of extent of cell depletion for tests designed to discharge the cells for times between 1 and 7 years. The discharge potential curves may be separated into two segments from $0 \leq x \leq \sim 0.51$ and $\sim 0.51 \leq x \leq 1.00$, where x is the dimensionless extent of discharge referenced to the rated cell capacity. The discharge potentials conform to Tafel kinetics in each segment. This behavior allows the discharge potential curves to be predicted for an arbitrary discharge load and long term discharge performance may be predicted from short term test results. The discharge potentials may subsequently be modeled by fitting the discharge curves to empirical functions like polynomials and Padé approximants. A function based on the Nernst equation that includes a term accounting for nonideal interactions between lithium ions and the cathode host material, such as the Redlich–Kister relationship, also may be used to predict discharge behavior.

1. Introduction

Implantable medical devices require an internal, autonomous energy source to function. Examples of such devices include implantable cardiac rhythm devices (pacemakers, cardioverter defibrillators and cardiac resynchronization devices) [1] neuromodulation devices and implantable drug pumps.

Cardiac rhythm devices treat patients with various cardiac conditions by applying electrical stimuli to heart tissue. A battery is the energy source for all device functions, including therapy, sensing and telemetric communication. Other types of power supplies were investigated, like nuclear and biological power sources, but are not considered to be as practical [2].

Lithium cells have been proven to be safe and reliable power sources for implantable cardiac rhythm devices since the 1970s [3]. A key determinant of battery electrical characteristics and discharge performance is the cathode material. A number of cathode materials have been used for implantable cardiac rhythm device batteries. Commonly used cathode materials today are iodine or carbon monofluoride (CF_x) for pacemakers and manganese dioxide (MnO_2) or silver vanadium oxide (SVO) for implantable defibrillators.

Implantable cardioverter defibrillator (ICD) devices have two basic therapeutic functions. They are pacemakers operating at relatively low power levels over long periods of time. They have the added capability of applying intermittent, high power electrical shocks to the heart to correct life threatening cardiac arrhythmias [1]. Cardiac resynchronization therapy defibrillator (CRT-D) devices have the same functions as ICDs, but also treat patients with heart failure.

ICDs and CRT-Ds are life sustaining devices. As a result, predicting the expected service life of the cell under disparate discharge conditions is important for patient safety. This requires a cell chemistry that is stable and reliable. Lithium cells using SVO cathode materials commonly have been used in ICDs since they were introduced in the 1980s and then, later, in CRT-Ds.

Manganese dioxide is an attractive cathode material as an alternative to SVO for powering implantable devices, including ICDs [4] and CRT-Ds. It has a high energy density useful for low power device operations, including cardiac pacing, and high rate capability to provide sufficient power for rapid delivery of high energy therapy shocks.

An extensive amount of work has been done to understand MnO_2 electrochemistry and to develop Li/MnO_2 cells for a variety of applications. MnO_2 was one of the first lithium cells using a solid cathode material to be commercialized. This chemistry has been used since the 1970s in consumer and OEM applications where high rate capability, chemical stability, reliability and longevity are required [5–7].

An example of a device that requires high reliability and longevity is the tire pressure monitor [8]. Serious accidents caused by underinflated tires prompted the recall of almost 6.5 million

* Tel.: +1 651 582 7974; fax: +1 651 581 3441.
E-mail address: michael.root@bsci.com.

0378-7753/$ – see front matter © 2010 Elsevier B.V. All rights reserved.
doi:10.1016/j.jpowsour.2009.12.083

tires in 2000. That same year, the US Congress enacted legislation requiring tire pressure monitoring systems in all US automobiles and light trucks.

Tire pressure monitors are pressure sensors that are mounted on each wheel rim of a vehicle. They must operate for up to 10 years under a wide range of unforgiving environmental conditions, including extreme temperatures (−40 to 120 °C), mechanical shock and vibration. Li/MnO_2 cells are used to power certain types of these sensors because they are capable of withstanding and operating in harsh conditions.

The US military recognizes the value of Li/MnO_2 batteries for applications like night vision goggles and emergency radio beacons [9] that require high reliability, rapid response after long periods of inactivity and the ability to function in a variety of environmental conditions.

The attributes described above suggest Li/MnO_2 cells would be practical for powering implantable medical devices. Merritt and Schmidt [10] explained the advantages of Li/MnO_2 cells for advanced implantable cardiac pacemakers that have power demands beyond the capability of the Li/I_2 cells that run most pacemakers today. In addition to rate capability, they commended the reproducible discharge behavior and predictable end of discharge characteristics of Li/MnO_2.

We describe how the discharge characteristics of Li/MnO_2 cells designed for ICD and CRT-D devices may be used to predict cell depletion.

2. Experimental

Cell description: Cells used in this study were designed for use in ICD and CRT-D devices. Hermetically sealed cells were assembled with lithium anodes and cathodes comprised of heat treated electrolytic MnO_2, carbon and polytetrafluoroethylene. The electrodes were assembled by alternatively stacking cathode and anode layers as generally described in a US patent [11].

Equipment: Fixed load discharge potentials were measured using an Fluke Hydra II 2620A data acquisition unit or National Instruments PXI-4106 multimeter. Pulses were applied using a Maccor BT4000 battery test system. Thermotron and Hotpack ovens maintained temperature control

Test Procedures: All tests were performed at 37 °C. Cells were discharged by attaching resistors to the cell terminals. Resistance values used were 14, 42, 75 and 113 kΩ and were selected to deplete the cells in 1, 3, 5 or 7 years. At 1- or 3-month intervals, depending on the total test time, 3.0 A pulses were applied to a constant energy end point of 50 J. A minimum of 4 cells were analyzed for each test level.

Calculations: Fits of functions to data were performed with Igor Pro 6.0.2.4 (WaveMetrics, Inc., Lake Oswego, OR, www.wavemetrics.com), which uses the Levenberg–Marquardt algorithm. Errors are given as $\pm 1\sigma$.

3. Results

Discharge test protocols for evaluating the performance of implantable defibrillator device cells are generally comprised of low rate, fixed load discharge for months to years with infrequent, high current pulses [12]. Li/MnO_2 cell discharge potentials during discharge at 1, 3, 5 and 7 y rates using fixed resistance loads are shown in Fig. 1.

The low discharge rates used allow us to assume:

1. Isothermal conditions.
2. Insignificant electrolyte mass transfer effects.
3. Homogeneous current distribution within the cathode.

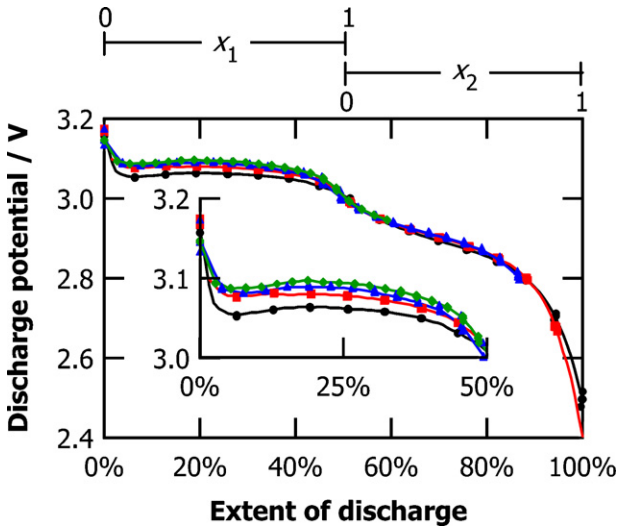

Fig. 1. Measured discharge potentials, E_{measd}, under different resistive loads at 37 °C with extent of discharge for Li/MnO_2 cells. Key to symbols: circles for the 1 y discharge rate, squares for the 3 y discharge rate, triangles for the 5 y discharge rate and diamonds for the 7 y discharge rate. The solid lines represent the means of interpolated discharge potentials. Inset: Expanded x_1 range plot of measured discharge potentials with extent of discharge.

4. Negligible polarization of the Li anode.

The last assumption above is supported by estimating a maximum polarization for the Li anode to be <1 μV using literature values for the exchange current density [13–15]. With these assumptions, changes in discharge potential are attributed to the electrochemical reactions of the MnO_2 cathode material.

The discharge potentials for Li/MnO_2 cells in Fig. 1 decrease with increasing discharge current (decreasing fixed load resistance) as a result of increased polarization. The characteristics of these discharge potentials are similar to those observed in previous studies [16–18]. The discharge potential curves may be separated into at least two distinct segments, from $0 \le x \le \sim 0.51$ and $\sim 0.51 \le x \le 1.00$, where x is the dimensionless extent of discharge referenced to the rated cell capacity. The extent of discharge within each of the two segments is calculated as $x_1 = x/0.51$ and $x_2 = (x - 0.51)/0.49$.

Internal ohmic resistance polarization at intervals throughout discharge was estimated from the initial voltage drop of the intermittent high current pulses by extrapolating the change in resistance with time to $t = 0$. Plots of the measured discharge potential, E_{measd}, at different depths of discharge corrected for iR loss, E_{-iR} against $\ln(E_{-iR}/R_L)$, where R_L is the fixed external load resistance, are linear (Fig. 2). The discharge current is calculated here by $i = E_{measd}/R_L$ or $i = E_{-iR}/R_L$ since the cell discharge was achieved using fixed load resistors rather than by constant current. This behavior suggests that MnO_2 discharge may be described by Tafel kinetics under the conditions used in this study.

The slopes of the lines in Fig. 2 are less than those observed for many simple electrochemical systems. For example, the slope of E_{-iR} against $\ln(E_{-iR}/R_L)$ is 35 mV per decade current at 26% depth of discharge and 18 mV per decade current at 76% depth of discharge. Low Tafel slopes were also observed for γ-MnO_2 in aqueous 5 mol dm^{-3} NH_4Cl with 2 mol dm^{-3} $ZnCl_2$ at pH5 (44 mV per decade current) [19] and in 9 mol dm^{-3} aqueous KOH solutions (35 mV per decade current) [20] at low current densities.

The maximum voltage correction for ohmic resistance is <1 mV for the low discharge rates used in this study so subsequent calculations were performed using measured discharge potentials, E_{measd}.

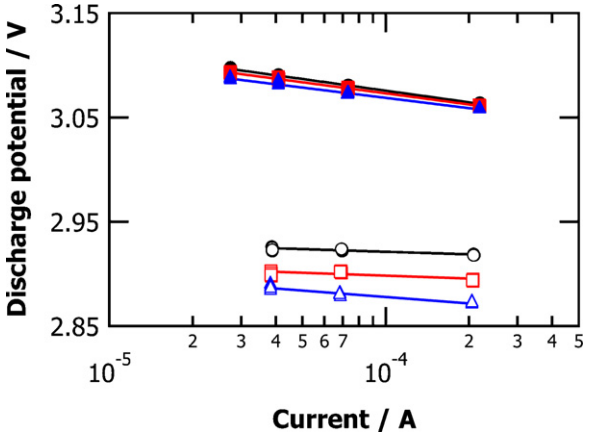

Fig. 2. Discharge potentials corrected for iR loss, E_{-iR}, under different fixed resistance loads (R_L) with extent of discharge for Li/MnO_2 cells plotted against the discharge current (E_{-iR}/R_L) on a logarithmic scale for the discharge potentials in Fig. 1. The discharge current is calculated as (E_{-iR}/R_L). Key to symbols: closed circles: 20% DOD, closed squares: 26% DOD, closed triangles: 32% DOD, open circles: 63% DOD, open squares: 70% DOD, open triangles: 76% DOD.

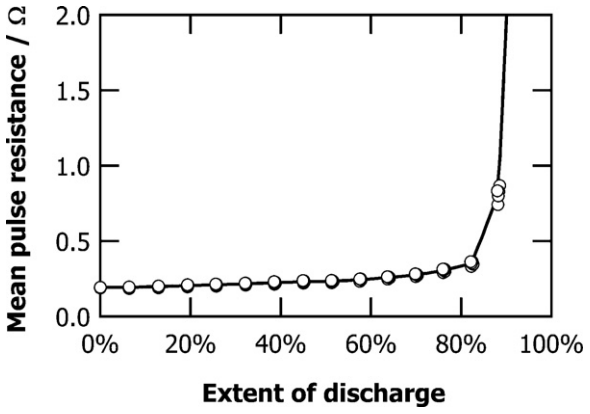

Fig. 3. Mean resistances for intermittent high current pulses drawn from Li/MnO_2 cells at 37 °C with extent of discharge for the 3 y discharge rate (circles) and mean of interpolated resistances (line).

The average pulse resistance shown in Fig. 3 for the intermittent, high current pulses is calculated by $(E_{prepulse} - E_{mean})/i$, where $E_{prepulse}$ is the potential just prior to the pulse (E_{measd}), i is the pulse current, which is constant, and E_{mean} is the mean potential for the pulse. This value is estimated by dividing the pulse energy in Wh by the pulse capacity in Ah. Pulse energy and capacity are reported by the cell test equipment software. The mean pulse resistance varies relatively little throughout discharge, until it increases when the battery is depleted, especially when compared to SVO discharge [12].

4. Discussion

As with any electrochemical power source, choice of cathode material is a key consideration for optimizing performance of implantable medical device cells. SVO has been used in implantable cardiac defibrillators since their introduction in 1985 and has helped millions of patients worldwide extend and enhance the quality of their lives. However, MnO_2 is a cathode material with attributes that are important for advanced cardiac rhythm devices.

When the internal resistance of a cell increases, polarization increases and has an effect on the high rate performance. This is consequential for defibrillator batteries that must be capable of delivering high current pulses. The resistance of SVO changes throughout discharge and is dependent on the rate of discharge [12]. Increasing cell resistance can be managed by increasing the number of high current pulses drawn from the cell [21], which removes additional capacity from the cell. Conversely, the internal resistance of Li/MnO_2 cells is relatively invariable through discharge and does not significantly increase until the battery is nearly depleted (Fig. 3).

Predictability of the discharge potential with extent of discharge under a wide range of discharge rates is central to determining expected device life. Although cells designed for ICD and CRT-D devices must be capable of providing high power on the order of watts, most of the discharge occurs at low power, typically in the microwatt range [1]. This means characterizing cell behavior at low discharge rates is necessary to understand cell performance and enable device longevity projections.

The measured discharge potential E_{measd} varies linearly with the logarithm of the discharge current, $\ln(E_{measd}/R_L)$, as seen in Fig. 2. As a result, the discharge potential may be calculated for an arbitrary load resistance. This also means the discharge potential characteristics of cells discharged at low currents in long term tests may be predicted from the discharge potentials of cells on shorter term discharge tests using the slope of the lines in Fig. 2 for each discharge segment.

The calculated discharge potential normalized to a reference discharge load, E_{calcd}, is estimated as $E_{calcd} = E_{measd} + RT/\alpha_c F \ln(R_{ref}/R_L)$ [22], where R is the gas constant, T is temperature, α_c is the transfer coefficient and F is the Faraday constant. The $RT/\alpha_c F$ term is the slope of E_{measd} vs. $\ln(E_{measd}/R_L)$. Arbitrary resistance R_{ref} is a fixed, external load selected for calculating the discharge potentials of a reference discharge test. The slopes of the E_{measd} vs. $\ln(E_{measd}/R_L)$ lines for both discharge segments in Fig. 1 used to calculate the discharge potentials at the reference load were -0.0155 V for $0 \le x_1 \le 1$ and -0.00677 V for $0 \le x_2 \le 1$.

Calculated discharge potentials for cells discharged at 1, 3 and 5 y rates adjusted to the 7 y discharge rate are shown in Fig. 4. The depth of discharge was further adjusted by 0.7% per year relative to the 1 year discharge rate to align the voltage curves. This adjustment may be considered to be an estimate of self-discharge valid for the data set used. Discharge potentials calculated as described previously in this section for tests lasting 1–5 years coincide with the 7 y discharge rate. These results indicate that long term discharge performance is readily predicted from shorter term testing [22].

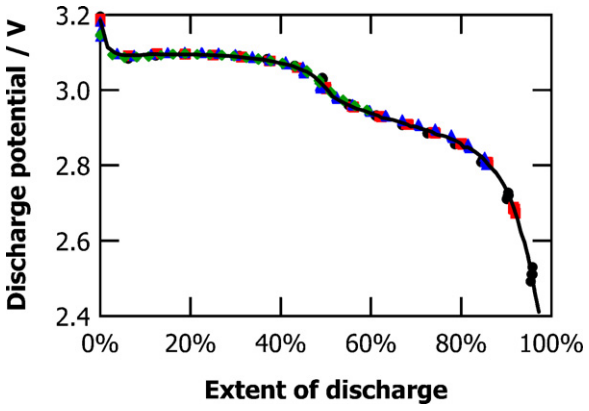

Fig. 4. Calculated discharge potentials at 37 °C, E_{calcd}, for Li/MnO_2 cells discharged at 1, 3 and 5 y rates normalized to the 7 y discharge rate and measured discharge potentials, E_{measd}, for cells discharged at the 7 y rate. Capacities are further adjusted for a constant 0.7% self-discharge per year relative to the 1 y discharge rate to align the voltage curves. Key to symbols: circles for the 1 y discharge rate, squares for the 3 y discharge rate, triangles for the 5 y discharge rate and diamonds for the 7 y discharge rate. The line represents the adjusted mean of interpolated discharge potentials for the 3 y discharge rate.

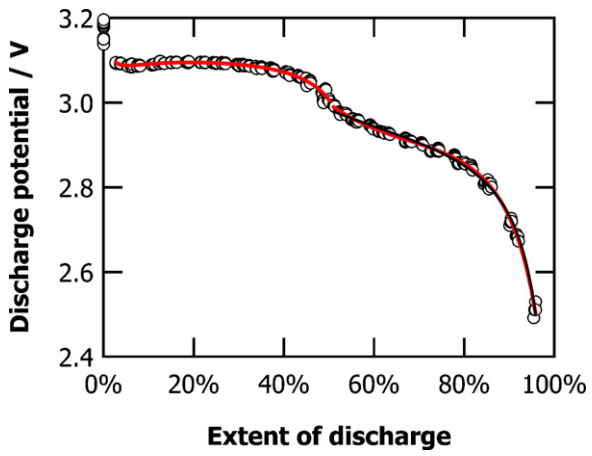

Fig. 5. Padé [3/3] functions (lines) for each segment $0.14 \le x_1 \le 1$ and $0 \le x_2 \le 1$ fit to the data in Fig. 4 (circles).

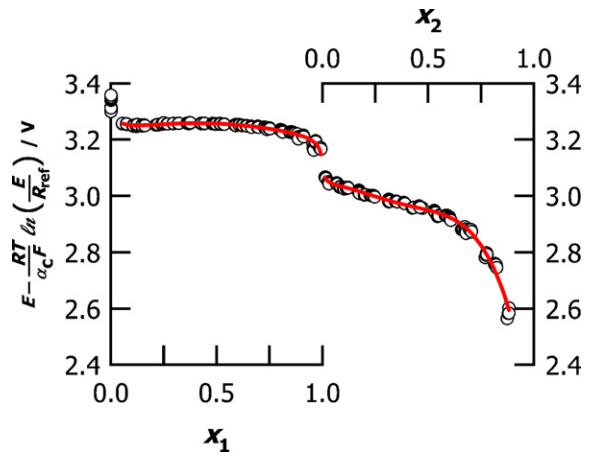

Fig. 6. Adjusted discharge potentials $[E - RT/\alpha_c F \ln(E/R_{ref})]$, calculated from the data in Fig. 4 (circles) with extent of discharge x_1 and x_2 and the corresponding fit lines corresponding to Eq. (3).

Discharge performance may be further characterized by finding an appropriate functional relationship between discharge potential and extent of discharge. Various empirical functions have been used to describe the equilibrium, or open circuit, potential of cells with extent of discharge [23,24]. These, or similar methods, such as rational functions like the Padé approximation [25], might be used to fit the normalized discharge curve for the results in Fig. 4. Padé [3/3] equations, $\left(\sum_{i=0}^{P} a_i x^i\right) / \left(1 + \sum_{j=1}^{Q} b_j x^j\right)$ with $P = 3$ and $Q = 3$, were used to fit the data in each segment $0.14 \le x_1 \le 1$ and $0 \le x_2 \le 1$ (Fig. 5). Values for the Padé coefficients are: $a_0 = 18.5 \pm 5.2$, $a_1 = 336 \pm 40$, $a_2 = 50.0 \pm 25.3$, $a_3 = -0.951 \pm 0.435$, $b_1 = 111 \pm 13$, $b_2 = 15.9 \pm 8.1$ and $b_3 = -0.302 \pm 0.139$ for $0.14 \le x_1 \le 1$ and $a_0 = 1770 \pm 97$, $a_1 = 2880 \pm 79$, $a_2 = 528 \pm 61$, $a_3 = -5.52 \pm 0.60$, $b_1 = 452 \pm 60$, $b_2 = 191 \pm 22$ and $b_3 = -1.92 \pm 0.21$ for $0 \le x_2 \le 1$.

Other functions may be used. The equilibrium potential for insertion compounds with extent of discharge has been described by variations of Eq. (1), wherein the equilibrium potential, E_{eq}, is a function the ratio of the concentrations of oxidized and reduced species.

$$E_{eq} = E^{0'} + \frac{RT}{nF} \ln\left(\frac{x_i}{1 - x_i}\right) + E_E(x_i) \quad (1)$$

In Eq. (1), $E^{0'}$ is the standard equilibrium potential for the experimental conditions, x_i is the fraction of discharged cathode material, x_1 or x_2, in either of the two segment observed in the discharge potential curve (Fig. 1), $(1 - x_i)$ is the corresponding fraction of discharged cathode material in each segment, n is the number of electrons participating in the electrochemical reaction and R, T and F have the meanings defined above.

Departure from ideal behavior has been attributed to excess free energy resulting from interactions between Li^+ and the host insertion compound. Including an interaction term, $E_E(x)$, in Eq. (1) accounts for these deviations by adjusting E_{eq} for nonideal activities. Several formulations for $E_E(x_i)$ in Eq. (1) have been used to represent the excess Gibbs free energy in mixtures as a function of x_i [26–28] including the Redlich–Kister relationship (Eq. (2)).

$$E_E(x_i) = \sum_{k=0}^{M} A_k \left[(2x_i - 1)^{k+1} - \frac{2kx_i(1 - x_i)}{(2x_i - 1)^{1-k}}\right] \quad (2)$$

where coefficients A_k are interaction parameters. Combining Eqs. (1) and (2) ($M = 3$ for $x_i = x_1$ and $M = 3$ for $x_i = x_2$) with the Tafel equation, $E = E_{eq} + (RT/\alpha_c F)\ln(i_0) - (RT/\alpha_c F)\ln(E/R_{ref})$ and setting $E = E_{measd}$ or E_{calcd} yields a function (Eq. (3)) for each segment $0 \le x_1 \le 1$ and $0 \le x_2 \le 1$ that adequately describes the discharge potential behavior with extent of discharge (Fig. 6).

$$E - \frac{RT}{\alpha_c nF} \ln\left(\frac{E}{R_{ref}}\right) = \text{constant} + \frac{RT}{nF} \ln\left(\frac{x_i}{1 - x_i}\right) + E_E(x_i) \quad (3)$$

The constant in Eq. (3) is $[E^{0'} + RT/\alpha_c F \ln(i_0)]$, which is used as a fit parameter here. Values for the Redlich–Kister coefficients are $A_0 = 0.0458 \pm 0.0006$, $A_1 = -0.0257 \pm 0.0010$, $A_2 = 0.00934 \pm 0.00129$, $A_3 = 0.00389 \pm 0.00200$ for $0.14 \le x_1 \le 1$ and $A_0 = -0.188 \pm 0.002$, $A_1 = -0.160 \pm 0.003$, $A_2 = -0.148 \pm 0.005$ and $A_3 = -0.102 \pm 0.006$ for $0 \le x_2 \le 1$.

5. Conclusions

The selection of Li/MnO_2 cells for use in implantable medical devices is driven by a number of factors. The electrochemical behavior of MnO_2 is well characterized and proven to be stable under diverse conditions.

The discharge characteristics of Li/MnO_2 are predictable, which is crucial for projecting cell service life in implantable medical devices. The Tafel behavior of Li/MnO_2 allows one to predict the behavior of longer term tests from the results of short term tests.

The discharge potentials may be modeled by fitting the discharge curves to a function that is based on determining the excess Gibbs free energy to account for nonideal interactions between lithium ions and the cathode host material or other empirical functions, such as polynomial equations or rational functions like Padé approximants.

Acknowledgement

We thank Ignacio Chi, Brian Schmidt and many others at Boston Scientific CRM for their important contributions to the development and testing of the cells used in this study.

References

[1] M.J. Root, J. Cardiovasc. Trans. Res. 1 (2008) 254–257.
[2] J.G. Webster (Ed.), Design of Cardiac Pacemakers, IEEE Press, New York, 1995.
[3] C.F. Holmes, in: K.M. Abraham, B.B. Owens (Eds.), Proc. Symp. Materials and Processes for Lithium Batteries 89-4, The Electrochemical Society, Pennington, NJ, 1989, pp. 42–55.
[4] J. Drews, G. Fehrmann, R. Staub, R. Wolf, J. Power Sources 97–98 (2001) 747–749.
[5] H. Ikeda, S. Narukawa, H. Nakashima, M. Fujimoto, in: A.N. Dey (Ed.), Proc. Symp. Lithium Batteries, 84-1, The Electrochemical Society, Pennington, NJ, 1984, pp. 311–322.
[6] D. Linden, Machine Des. 58 (1986) 134–135.
[7] H. Ikeda, J. Electron. Eng. 18 (1981) 40–44.

[8] T. Desai, K. Chance, T. Ozawa, RFDesign (2004) 50–56.
[9] M.C. Hart, E.P. Thurston, W. Andruk, T.B. Reddy, Proceedings of the IEEE 35th International Power Sources Symposium, 1992, pp. 129–132.
[10] D.R. Merritt, C.L. Schmidt, in: S. Surampudi, V. Koch (Eds.), Proc. Symp. Lithium Batteries, 93-24, The Electrochemical Society, Pennington, NJ, 1993, pp. 138–145.
[11] M.J. O'Phelan, T.G. Victor, B.J. Haasl, L.D. Swanson, R.J. Kavanagh, A.G. Barr, R.M. Dillon, US patent 7,479,349.
[12] A. Crespi, C. Schmidt, J. Norton, K. Chen, P. Skarstad, J. Electrochem. Soc. 148 (2001) A30–A37.
[13] S.G. Miebuhr, J. Electrochem. Soc. 117 (1970) 56–60.
[14] R.F. Scarr, J. Electrochem. Soc. 117 (1970) 295–299.
[15] S.G. Miebuhr, J. Electrochem. Soc. 118 (1971) 1320–1322.
[16] Y. Shao-Horn, S.A. Hackney, B.C. Cornilsen, J. Electrochem. Soc. 144 (1997) 3147–3153.
[17] T. Ohzuku, M. Kitagawa, T. Hirai, J. Electrochem. Soc. 136 (1989) 3169–3174.
[18] J.C. Nardi, J. Electrochem. Soc. 132 (1985) 1787–1791.
[19] A. Kozawa, R.A. Powers, Electochem. Technol. 5 (1967) 535–542.
[20] A. Kozawa, R.A. Powers, J. Electrochem. Soc. 115 (1968) 122–126.
[21] H. Gan, N. Waite, K. Syracuse, E.S. Takeuchi, US patent 7,375,496.
[22] S. Davis, E.S. Takeuchi, W. Tiedemann, J. Newman, J. Electrochem. Soc. 154 (2007) A477–A480.
[23] T.F. Fuller, M. Doyle, J. Newman, J. Electrochem. Soc. 141 (1994) 1–10.
[24] Q. Guo, R. White, J. Electrochem. Soc. 152 (2005) A343–A350.
[25] E. Hernandez-Pacheco, M.D. Mann, J. Power Sources 128 (2004) 25–33.
[26] D.K. Karthikeyan, G. Sikha, R.E. White, J. Power Sources 185 (2008) 1398–1407.
[27] M. Jain, A.L. Elmore, M.A. Matthews, J.W. Weidner, Electrochim. Acta 43 (1998) 2649–2660.
[28] J.M. Prausnitz, Molecular Thermodynamics of Fluid Phase Equilibria, Prentice-Hall, Princeton, NJ, 1986, pp. 213–299.